Waters™

应用纪要

Beyond Dye-Based Encapsulation Assays: Multi-attribute Quantification of Anti-CD3 Conjugated In Vivo CAR-T Type LNPs by FFF-MALS, DLS, and ELS

Martin Kurnik, Mateusz Imiołek, Matthew Lauber, Michelle Chen

Waters Corporation, United States

Published on November 26, 2026

Abstract

Lipid nanoparticles (LNPs) show promise in a wide range of therapies. Compared to the first successful LNP drug products that targeted amyloidosis and COVID-19, next generation applications such as *in vivo* CAR-T therapy are more challenging to develop. For example, a widely pursued strategy to achieve delivery specificity of next-generation LNP drug products is to conjugate targeting moieties such as antibodies, peptides, or nucleic acids to the LNPs. The resulting "targeted" LNPs (tLNPs) are often heterogeneous products demanding more complex purification and characterization than LNPs made from only lipids and drug substance.

This application note demonstrates high-resolution multi-attribute quantification (MAQ) of tLNPs by field-flow fractionation coupled to multi-angle light scattering detection (FFF-MALS), including quantification of the number of antibody ligands per LNP. The results are compared to low-resolution screening by dynamic light scattering (DLS) and electrophoretic light scattering (ELS), demonstrating

that FFF-MALS is a superior solution for in-depth characterization in development, manufacturing, and quality control of tLNP drug products.

Benefits

- DynaPro™ ZetaStar™ enables automated screening of particle size, polydispersity, and zeta potential
- FFF-MALS provides multi-attribute quantification of particle size, molecular weight (MW), and payload distribution
- FFF-MALS also measures dispersity (M_w/M_n), a parameter that has been shown to correlate with LNP-mRNA bioperformance
- Additionally, FFF-MALS can resolve free monoclonal antibodies (mAbs) from mAb-targeted mRNA-LNPs, enabling quantification of the average number of mAbs per LNP particle

Introduction

Lipid nanoparticles (LNPs) show potential across a wide range of therapies, with next-generation applications including CRISPR gene editing, autoimmune disease treatment, cancer immunotherapy, and in vivo CAR-T cell therapy. These applications do, however, pose more formidable challenges in terms of delivery, biodistribution, persistence, immunogenicity, gene expression, safety, and efficacy than the LNP-mRNA drug products that are currently approved by regulatory agencies.[1] Numerous LNP drug products in development employ site-specifically conjugated targeting ligands proven in other contexts, such as antibodies, sugars, peptides, or nucleic acids, to the LNPs. The bioconjugation chemistries used to generate these so-called decorated, conjugated, or targeted LNPs (tLNPs) typically yield heterogeneous products and the LNP surface may be coated with a mixture of site-specifically conjugated and non-specifically adsorbed, partially buried, or non-functional, ligand. Consequently, the complex chemistry of the resulting drug product demands additional purification and more involved, high-resolution quantification of multiple attributes by orthogonal techniques for rigorous manufacturing and quality control, including assessment of purity, residual amounts of free ligand, and ligand density.

This application note demonstrates how field-flow fractionation coupled to multi-angle light scattering

(FFF-MALS) can be used for both separation and high-resolution multi-attribute quantification (MAQ) of tLNPs. The combination of MALS and differential refractive index (dRI) and UV/vis absorbance concentration detectors enable quantification of multiple key LNP attributes, including size, molar mass, and payload distributions, polydispersity, encapsulation efficiency, conjugation yield, residual free ligand concentration, and ligand density for particles with up to two micron diameter. Attributes may be evaluated across the entire sample or specific subpopulations.

FFF-MALS provides a gentle, size-based separation solution for large, shear-sensitive particles that adsorb to size-exclusion chromatography (SEC) columns or exhibit other non-ideal elution behavior. Since FFF separation is tunable, a single FFF experiment also provides quantification across a broader size range than SEC. For tLNPs, FFF can be used to resolve and quantify free ligand and payload, as well as the intact LNPs in a single experiment. tLNP SEC, in contrast, typically requires patching together results from multiple columns and experiments to optimally resolve the different species due to their large size difference, and non-ideal SEC separation and column interactions may still prevent accurate quantification and result in poor mass recovery. The combined batch batch dynamic and electrophoretic light scattering (DLS and ELS, respectively) and FFF-MALS workflow presented here provides a comprehensive solution for tLNP characterization, from rapid, low-resolution screening to in-depth, high-resolution multi-attribute quantification. FFF-MALS measurements are also non-destructive, and subpopulations may be fractionated and recovered from the experiment by fraction collection for further evaluation by offline orthogonal assays.

Experimental

Sample Description

RNA-loaded LNP-RNA formulations and an empty LNP control sample were kindly provided by Phosphorex LLC (Hopkinton, MA). The LNP-RNA samples incorporated 0–5% dibenzo-cyclooctyne (DBCO) to facilitate click-chemistry surface conjugation with an azide-modified anti-CD3 monoclonal antibody (mAb). Final conjugated mAb concentrations of the four LNP-RNA samples were 0, 0.06, 0.16, and 0.34 mg/mL, respectively. The untargeted empty LNP control sample (0% DBCO) was prepared in 10 mM citrate buffer, pH 3.0. All final LNP formulations were maintained in a storage buffer consisting of 20 mM Tris-HCl, pH 7.4 and 8% (w/v) sucrose.

Dynamic and Electrophoretic Light Scattering

Samples were diluted 5-fold in 12 mM phosphate, pH 7.4, i.e., phosphate-buffered saline (PBS) excluding NaCl and KCl and measured in a quartz cuvette at 25 °C with the DynaPro ZetaStar Instrument. While these samples use a low-ionic strength formulation buffer, measurements may also be made at higher ionic strength with a pressurized flow cell and automation if desired.[2] Data analysis was performed with DYNAMICS™ Software. Reported averages and standard deviations are from six replicate measurements for size and polydispersity and three replicate measurements for zeta potential.

Field-flow Fractionation with UV-MALS-dRI Detection

FFF-MALS measurements were performed on an Eclipse™ FFF instrument with a 350 µm fixed-height short channel connected to a Waters Arc™ HPLC System with a Quaternary Solvent Manager (QSM) pump and a Sample Manager Flow-Through Needle-R (FTN-R). A DAWN™ MALS Photometer, an Optilab™ differential refractometer, and a 2998 PDA Detector set to 260 nm wavelength were used for online detection. Online fluorescence detection may also be employed if desired. The FFF system was controlled by VISION™ Software. Data acquisition and analysis were performed in ASTRA™ Software.

The samples were measured neat, without any additional preparatory steps. The FFF method was a starter method for LNP separation provided with the Eclipse FFF instrument and used as-is, without any need for method development and optimization. The mobile phase was PBS, pH 7.4. Generally, FFF-MALS analysis can be done directly in typical LNP formulation buffers like Tris, PBS, or other commonly used buffers for biomolecules such as Good' s buffers[3] with or without added salt and without need for buffer exchange prior to the analysis. Reported averages and standard deviations are from three replicate injections.

Empty LNP samples with lipid compositions matching the loaded LNP samples were also measured with the same FFF method as the loaded LNP samples, and the results were used to generate experimentally derived UV scattering correction profiles with ASTRA LNP Analysis Module Software. These correction profiles were applied to the measurement results from the loaded LNP samples to obtain accurate payload and particle concentrations non-destructively.

FFF Conditions

LC system:	Arc HPLC System

FFF instrument:	Eclipse with Dilution Control Module (DCM)
Detection:	DAWN MALS Photometer Optilab differential Refractometer 2998 PDA Detector, collecting UV absorbance at 260 nm
Vials:	Waters Clear Glass Screw Neck Total Recovery Vials, 12 x 32 mm
Channel:	350 µm fixed-height short channel
Channel temperature:	Ambient
Sample temperature:	4 °C
Injection volume:	25–30 µL
FFF method:	Eclipse FFF starter method for tLNPs
Detector flow rate:	0.50 mL/min
Mobile phase:	PBS, pH 7.4 (10 mM Na_2HPO_4, 1.8 mM KH_2PO_4, 137 mM NaCl, 2.7 mM KCl)

Data Management

FFF control:	VISION 4 Software
Data collection and analysis:	ASTRA 8 Software

Results and Discussion

LNP Size Screening and High-precision Zeta Potential Determination

Batch DLS and ELS were used to screen the size distribution and zeta potential of both the bare LNPs and the anti-CD3 mAb-conjugated tLNPs ahead of the FFF-MALS measurements. Batch DLS measurements are fast, making the technique an excellent pre-screening complement to higher-resolution techniques like FFF-MALS, mass spectrometry, and electron microscopy. As seen from the results, however, batch DLS cannot replace high-resolution tools for comprehensive LNP characterization, especially in the context of tLNPs.

The average size measured by batch DLS has low resolution as shown in Figure 1 and Table 1, and species that are <3-5-fold different in size cannot be resolved. This limitation is most clearly seen for the lot-certified bovine serum albumin standard in Figure 1, that appears to contain a single population without resolving the monomers from the oligomers known to be present in the sample from the MALS results in the standard’ s certificate of analysis.

Batch DLS also struggles to accurately quantify the LNP size distributions, as the samples are polydisperse and the particles are large enough to scatter more light in the forward direction relative to the laser light source in a size-dependent manner. Consequently, LNP size measured by batch DLS generally depends on the measurement angle (Table 1), whereas this effect is negligible for small, predominantly monodisperse samples such as BSA. The bare LNP sample without antibodies conjugated to the particles appeared to contain a single, polydisperse LNP population (Figure 1), with an average hydrodynamic radius (R_h) of 52.2 ± 0.8 nm measured from side-scattering, and 43.8 ± 0.4 nm from back-scattering. The lowest DBCO and mAb concentration used for conjugation increased the average R_h by 20-30 nm (Table 1). Inspecting the size distribution, conjugation appeared to increase the size of some of the particles. Increasing the DBCO and mAb concentration further, the size distribution became even wider and progressively more skewed towards larger particles. The discrepancy between the size from side-scattering and back-scattering angles also increased with particle size; up to ~40% at the highest mAb concentration (Table 1).

The zeta potential of the unconjugated LNPs was slightly negative, at -15.6 ± 1.1 mV. As the mAb concentration in the sample increased, zeta potentials approached zero, potentially impacting LNP stability and amenability to cellular uptake. As inter-particle interactions are a function of surface

charge, the reduction in zeta potential upon conjugation may be facilitating the formation of the larger particles seen in the tLNP samples.

No free mAb was detected in any of the tLNP samples. When interpreting this result, however, it is important to keep in mind that all batch DLS instruments measure intensity distributions rather than mass distributions. The relative signal contribution from a particle increases with its size, and the intensity distributions are dominated by the LNPs. The LNP signal may even completely mask the signal from low concentrations of small particles like free ligand in a tLNP sample. As seen below, a higher-resolution technique like FFF-MALS is required to detect and quantify the free mAb in tLNP samples while also enabling more in-depth characterization of the tLNP population.

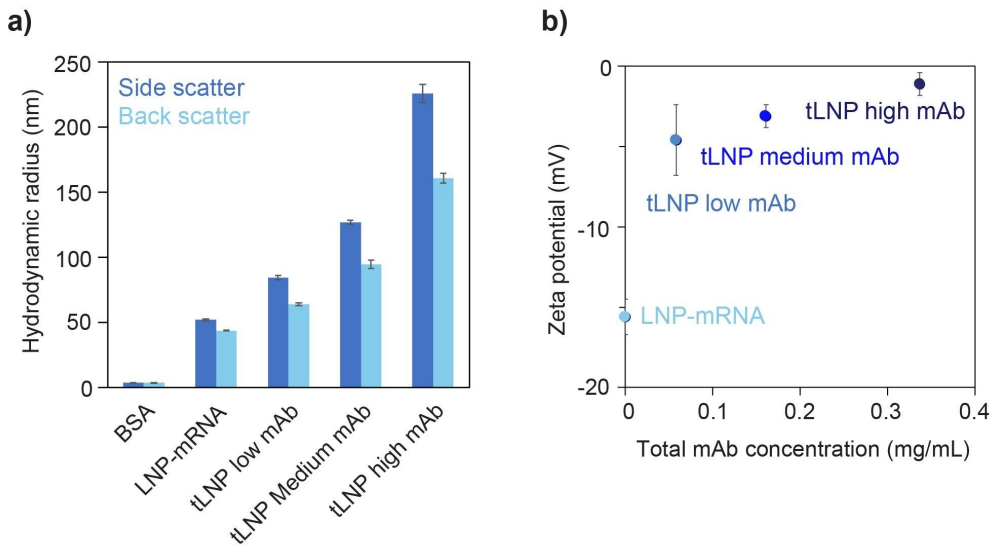


Figure 1. tLNP samples analyzed by dynamic light scattering (DLS) and electrophoretic light scattering (ELS). a) Low-resolution size from DLS. The measured size depends on the measurement angle. All LNPs are larger than the bovine serum albumin (BSA) standard included for reference (R_h = 3.7 nm). b) The average LNP zeta potential decreases in magnitude as a function of the mAb concentration used for the conjugation reaction, resulting in effectively neutral particles at the highest mAb concentration.

Sample	Total mAb conc. (mg mL^{-1})	R_h (nm)[a]	PDI[a]	R_h (nm)[a]	PDI[a]	Zeta potential (mV)[b]
		Detection angle: 90 degrees		Detection angle: 163.5 degrees		
BSA	–	3.72 ± 0.02	0.10 ± 0.02	3.74 ± 0.02	0.10 ± 0.02	N.D.
Empty	–	69.0 ± 0.7	0.40 ± 0.02	46.2 ± 0.5	0.31 ± 0.01	N.D.
LNP-RNA	–	52.2 ± 0.8	0.30 ± 0.02	43.8 ± 0.4	0.19 ± 0.02	-15.6 ± 1.1
tLNP low mAb	0.06	84.5 ± 1.5	0.34 ± 0.02	64.1 ± 0.9	0.27 ± 0.01	-4.6 ± 2.2
tLNP medium mAb	0.16	127.0 ± 1.5	0.34 ± 0.01	94.7 ± 3.2	0.34 ± 0.01	-3.1 ± 0.7
tLNP high mAb	0.34	225.8 ± 7.1	0.42 ± 0.02	160.7 ± 3.8	0.44 ± 0.02	-1.1 ± 0.7

Table 1. LNP size, polydispersity index, and zeta potential from batch DLS and ELS. [a] Averages and standard deviations from six replicate measurements. [b]Averages and standard deviations from three replicate measurements.

Multi-Attribute Quantification and Payload Analysis by FFF-MALS

FFF-MALS separates and quantifies tLNPs and residual free ligand in a single experiment and provides higher-resolution quantification than batch DLS (Figure 2).

The unconjugated LNP-RNA sample (Figure 2, light blue trace) contained a single, polydisperse LNP population with an average radius of 45.8 ± 1.8 nm, in good agreement with the result from the lower-resolution DLS measurement (Table 1). In contrast to batch DLS, however, FFF-MALS experiments also measure mass concentration, providing high-resolution quantification of the mass fraction of differently sized particles in (t)LNP samples (Figure 2b), weight-average molar mass (M_w), and true IUPAC dispersity, defined as the ratio of the weight-average and number-average molar mass (Table 2). The LNP dispersity from FFF-MALS can be a more accurate predictor for LNP performance in biological models than the size or polydispersity index calculated from DLS data[4]. The unconjugated RNA-LNPs (light blue trace in Figure 2) had a weight-average molar mass of 76.2 ± 1.4 MDa and a polydispersity of 1.26 ± 0.03, and the LNP concentration in the sample was 2.0 × 10^{13} particles/mL. The same experiment also quantified the total, lipid, and payload molar mass and concentration across the peak (Figure 2c, Table 3). The LNPs had an average nucleic acid weight fraction (F_w NA) of 4.9 ± 0.1 %, and an encapsulation efficiency of 99 ± 1 %. Should it be of interest, the payload content can also be analyzed as a function of particle size, to quantify the amounts of particles with a specific size and payload content.[5]

Adding DBCO and mAb to the LNP-RNA particles to enable conjugation, a population of larger LNPs appeared as a shoulder on the tail end of the LNP peak in the fractograms (Figure 2a), reducing the relative amount of the original LNP population in favor of larger particles (Figure 2b). Even the lowest mAb and DBCO concentration gave a pronounced increase in average size, molar mass, and dispersity, and the particle concentration consequently also decreased (Table 2). Increasing the mAb and DBCO concentration further skewed the size distribution toward larger particles. There were no substantial differences in overall nucleic acid weight fraction or encapsulation efficiency between the different samples, suggesting that encapsulation was uncoupled from conjugation. This is as expected, given that the LNP-RNA particles for all samples were manufactured by the same mixing process, followed by conjugation. The total LNP dRI peak area was also effectively identical across all samples (6% standard deviation), supporting that conjugation does not compromise mass recovery. The close overlap of the molar mass distributions and average encapsulation efficiencies of the different samples also indicated that the mAb only contributed 3% or less to the overall tLNP particle mass in the tLNP samples.

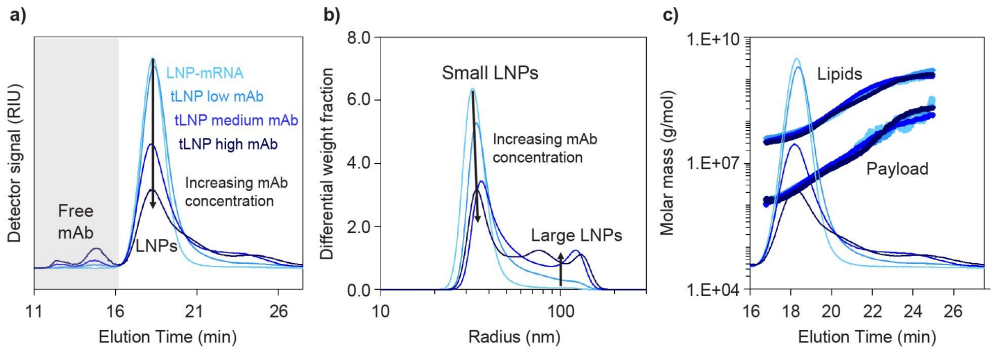


Figure 2. FFF-MALS separation and quantification of the LNP-RNA and tLNP samples. a) dRI fractograms. Both the LNPs and free mAb ligand were resolved and quantified in a single experiment. b) Mass fractions measured by FFF-MALS-UV-dRI for the different LNP populations. Conjugation converts part of the original LNP-RNA population into larger LNPs. c) FFF-MALS payload analysis.

Sample	Total mAb conc. (mg mL^{-1})	R_z (nm)	M_w (MDa)	$Đ = M_w/M_n$	Particle conc. (× 10^{13} mL^{-1})[a]
LNP-RNA	–	45.8 ± 1.8	76.2 ± 1.4	1.26 ± 0.03	2.00 ± 0.03
tLNP low mAb	0.06	81.7 ± 4.7	124.9 ± 8.0	1.74 ± 0.08	1.60 ± 0.02
tLNP medium mAb	0.16	94.2 ± 1.5	231.7 ± 6.6	3.00 ± 0.11	1.18 ± 0.04
tLNP high mAb	0.34	109.9 ± 3.4	263.4 ± 22	3.68 ± 0.25	0.94 ± 0.03

Table 2. FFF-MALS multi-attribute quantification of the LNP-RNA and tLNP samples. Averages and standard deviations of three replicate measurements for the peak range in Figure 2c.

Sample	Total mAb conc. (mg mL^{-1})	Lipid conc. (mg mL^{-1})	Payload conc. (mg mL^{-1})	F_w Payload
LNP-RNA	–	1.91 ± 0.03	0.099 ± 0.001	0.049 ± 0.001
tLNP low mAb	0.06	1.81 ± 0.03	0.098 ± 0.003	0.052 ± 0.002
tLNP medium mAb	0.16	1.44 ± 0.01	0.076 ± 0.004	0.050 ± 0.002
tLNP high mAb	0.34	1.05 ± 0.03	0.068 ± 0.002	0.061 ± 0.003

Table 3. LNP payload analysis results. Averages and standard deviations of three replicate measurements for the peak range in Figure 2c.

Quantification of tLNP Ligand Conjugation by FFF-MALS

FFF-MALS can also be used to quantify the residual concentration of free ligand, the number of mAbs per LNP as a function of *e.g.,* particle size or the total mAb concentration from manufacturing, and to estimate the ligand density on the particle surface for tLNP samples. For example, FFF-MALS-UV-dRI resolved and quantified the amount of free mAb (Figure 2; the first peak corresponds to monomer and the second to dimer) and the LNP concentration (Table 2) in the three tLNP samples, and the total mAb amount in the tLNP sample is typically known from orthogonal experiments, such as batch UV/vis

absorbance measurements or SEC under deformulating conditions. Combining such data enables easy evaluation of the number of mAbs per LNP as a function of *e.g.,* the mAb concentration or LNP size (Figure 4). For the tLNP samples in this study, the amount of residual free mAb was ~40% at all mAb concentrations. The number of mAbs per LNP, in contrast, increased with mAb concentration and average particle size. Specifically, the tLNPs generated with the lowest mAb and DBCO concentration had an estimated average of 9 mAbs/LNP, and this number increased up to >80 mAbs/LNP for the sample with the highest mAb and DBCO concentration. While this last number may appear high, it was an average across the tLNP peak. Consequently, the average number reflects that the mass fraction of very large particles increases with DBCO/mAb concentration (Figure 2, Table 1). For tLNP samples, mAbs may be confined to the LNP surface by a combination of site-specific conjugation and non-specific adsorption (NSA), i.e., the number of mAbs per particle may not be limited by the number of conjugation sites, but rather the LNP surface area. The ~50 nm average radius of the unconjugated LNP-RNA particles used as starting material for the conjugation reaction corresponds to a surface area of ~3×10^4 nm^2: large enough to potentially accommodate up to ~400 mAbs per particle.

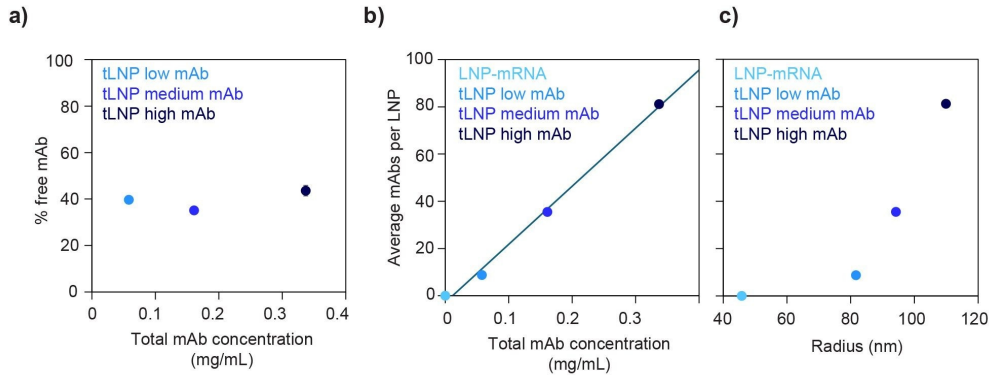


Figure 3. FFF-MALS can be used to estimate a) residual amounts of free mAb as well as the number of mAbs per LNP as a function of b) mAb concentration and c) average particle size.

Consistent with that mAb conjugation does not appear to substantially impact the LNP nucleic acid weight fraction or encapsulation efficiency, there also did not appear to be any significant change in the hydrodynamic radius of the main population upon conjugation (Figure 4a), supporting that the FFF separation of these samples was ideal i.e., based on particle size. That said, the RMS radius measured in

the same FFF-MALS experiment appeared to increase with mAb concentration, suggesting that the particle mass distribution shifted further away from the particle center of mass as a function of the mAb concentration used for the conjugation reaction (Figure 4b). The RMS radius increase may reflect rearrangements in the particle or morphological changes associated with mAb conjugation to the particle surface. The phenomenon may also be captured as the ratio of the RMS radius to the hydrodynamic radius (Figure 4c).

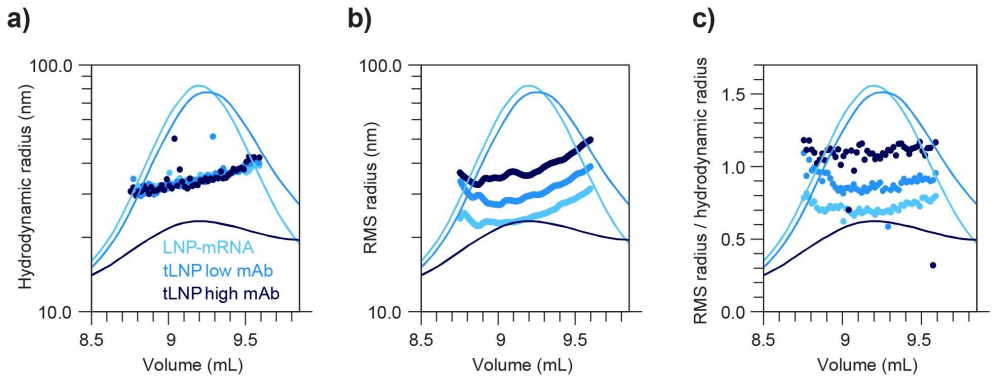


Figure 4. Comparison of a) the hydrodynamic radius and b) the RMS radius of the unconjugated and mAb-conjugated LNPs suggests mAb conjugation induces a structural evolution in the LNPs that becomes more pronounced at higher mAb concentration. This phenomenon may also be described by c) the ratio of the RMS radius to the hydrodynamic radius.

Note that the example above is a simple proof-of-principle experiment. If desired, more refined analysis of subfractions of the LNP peak corresponding to specific subpopulations recovered by fraction collection may also be performed using common orthogonal techniques. For example, chromatography under deformulating conditions that disrupt the LNPs[6, 7] may be used as a second-dimension method for quantifying the total mAb and nucleic acid concentrations in different LNP subpopulations recovered from the FFF experiment using *e.g.,* the Waters WFM-A fraction manager.

Conclusion

This application note demonstrates how FFF-MALS can be used for high-resolution multi-attribute quantification of both tLNPs and two-component RNA-LNPs. The results presented here were obtained using mAb-conjugated LNPs and the analysis workflow is also compatible with LNPs conjugated to other targeting moieties such as nanobodies, sugars, or oligonucleotide aptamers. Because FFF-MALS is non-destructive, the technique may also be applied to LNPs exposed to biological sample matrices like serum or plasma. In such experiments, the LNPs are first separated by size using FFF, followed by characterization of the particles and protein corona by MALS-UV-dRI and orthogonal techniques such as mass spectrometry, flow cytometry, dye-binding fluorescence assays, size-exclusion chromatography under deformulating conditions, or other chromatography modes. FFF-MALS also provides higher-resolution, more accurate, and more comprehensive tLNP characterization than batch DLS, making FFF-MALS the superior tool for high-resolution multi-attribute characterization of tLNP samples from development to manufacturing and quality control.

References

1. Geisler, H.C.; *et al.* Resolving Heterogeneity of Targeted Lipid Nanoparticles Through Solution-Based Biophysical Analyzes. Adv. Mater. 38(48), e73984 (2026).
2. Kurnik, M.; *et al*. AN6004: Automated, High-Precision Liposome Zeta Potential Measurements at High and Low Salt Concentrations <https://wyattfiles.s3.us-west-2.amazonaws.com/literature/app-notes/dls-plate/AN6004_Automated_High-Precision_Liposome_Zeta_Potential_Measurements_at_High_and_Low_Salt_Concentrations.pdf> . Waters Application Note (2026).
3. Ferguson, W.J.; *et al.* Hydrogen Ion Buffers for Biological Research. *Anal. Biochem.* 104(2),300 (1980).
4. Padilla, M.S.; *et al*. Elucidating Lipid Nanoparticle Properties and Structure Through Biophysical Analyzes. *Nat. Biotechnol.* 44(9),1502 (2026).
5. Kurnik, M.; AN2615: Multi-attribute Quantification of LNP-mRNA Therapeutics by FFF-MALS and DLS < https://wyattfiles.s3.us-west-2.amazonaws.com/literature/app-notes/fff-mals/AN2615-Multi-attribute-quantification-of-LNP-mRNA-theraputics-by-FFF-MALS-and-DLS.pdf> . Waters Application Note (2024).

6. Imiolek, M.; *et al*. High-Throughput Quantification and Characterization of Dual Payload mRNA/LNP Cargo via Deformulating Size Exclusion and Ion Pairing Reversed Phase Assays. *Anal. Chem.* 97(5),3091 (2025).

7. Imiolek, M.; *et al.* Beyond Dye-Based Encapsulation Assays: Multi-attribute quantification of anti-CD3 conjugated in vivo CAR-T type LNPs by Deformulating SEC and FFF-MALS. Waters Application Note (2026). Available online at www.waters.com <http://www.waters.com> .

Acknowledgements

We thank Evan Turek, Nicholas Boylan, Matthew Freeman, Chelsea Johnson, Theresa Logan, Irodiel Vinales, and Saher Abu Aita at Phosphorex LLC for preparing the samples and scientific discussions.

Featured Products

Arc HPLC System <https://www.waters.com/nextgen/global/products/chromatography/chromatography-systems/arc-hplc-system.html>

DAWN <https://www.wyatt.com/products/instruments/dawn-multi-angle-light-scattering-detector.html>

Eclipse <https://www.wyatt.com/products/instruments/eclipse-field-flow-fractionation-system.html>

ASTRA 8 <https://wyatttechnology.zendesk.com/hc/en-us/articles/360052705793-ASTRA-8>

VISION 4.4 <https://wyatttechnology.zendesk.com/hc/en-us/articles/29197220101779-VISION-4-4>

720009768, November 2026

© 2026 Waters Corporation. All Rights Reserved.

使用条款 隐私声明 商标 招聘 法律和隐私声明 危险化学品经营许可证 Cookie Cookie设置 请勿出售我的个人信息
沪ICP备06003546号-2 京公网安备 31011502007476号 药品医疗器械互联网信息服务备案编号: 沪网药械信备字[2026]000045号